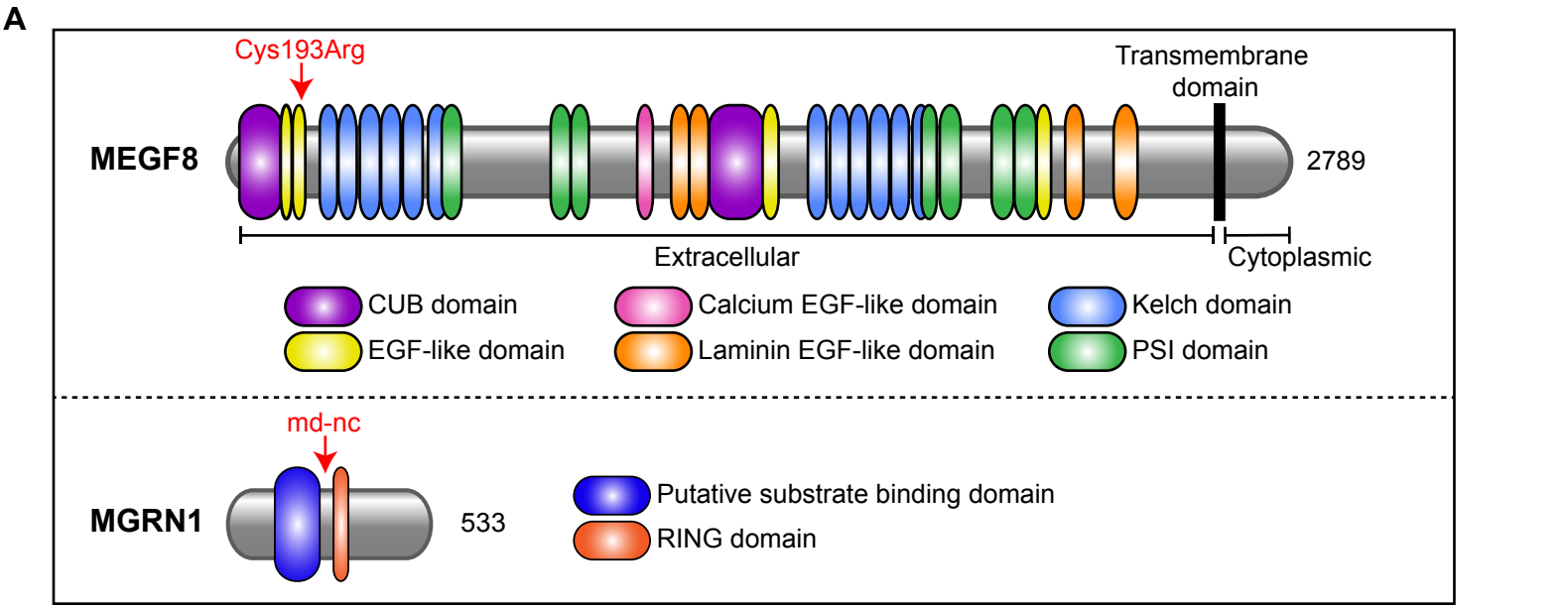

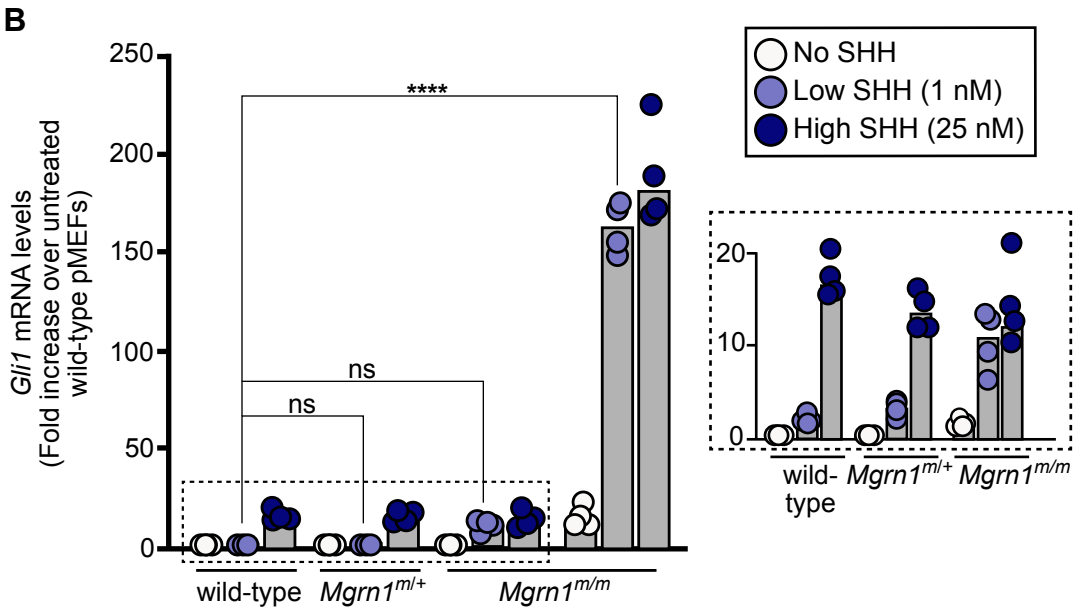

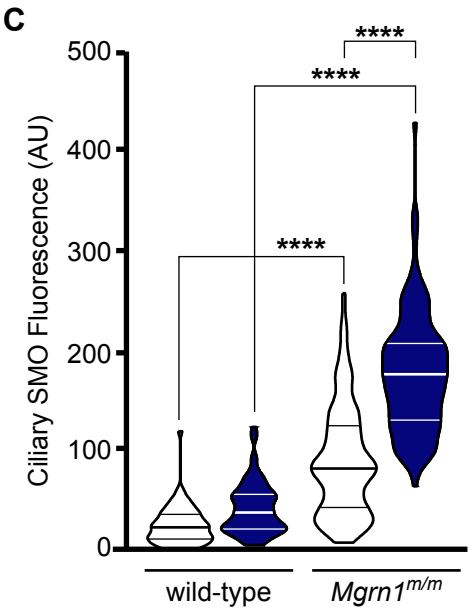

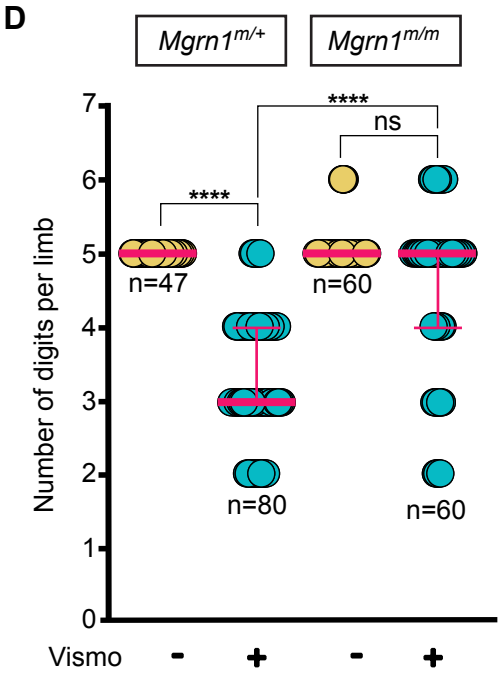

E

Genotype	Digits per limb Median (interquartile range)
Mgrn1$^{m/+}$	5 (5, 5)
Mgrn1$^{m/+}$ + Vismo	3 (3, 4)
Mgrn1$^{m/m}$	5 (5, 5)
Mgrn1$^{m/m}$ + Vismo	5 (4, 5)

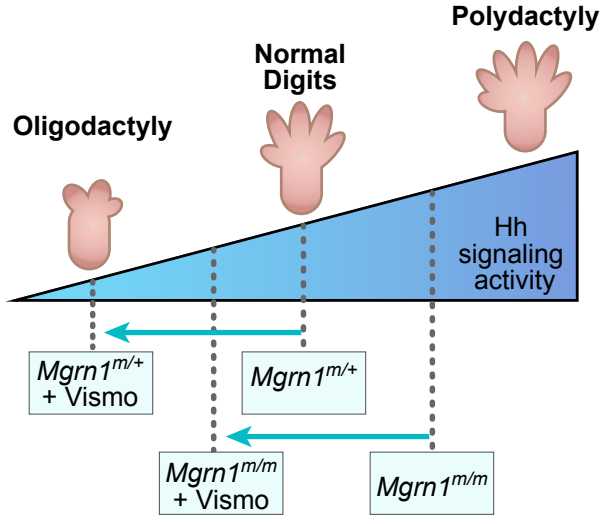

Figure S1. Related to Figure 1: Elevated Hh signaling in *Mgrn1*$^{m/m}$ cells and embryos.

(A) Domain composition of mouse MEGF8 and MGRN1 (UniProt Consortium, 2019). The arrow above MEGF8 denotes the location of the missense mutation (C193R) in the second EGF-like domain of MEGF8 (Zhang et al., 2009) that causes heart defects and heterotaxy in mice. In the loss-of-function *md-nc* allele of *Mgrn1*, a thymidine to adenine mutation in intron 9 disrupts splicing, leading to a premature stop (at the position shown by the arrow above MGRN1) and nonsense mediated decay of the transcript (He et al., 2003).

(B) Hh signaling strength was assessed using qRT-PCR to measure *Gli1* mRNA in primary mouse embryonic fibroblasts (pMEFs) prepared from wild-type, *Mgrn1*$^{m/+}$, and *Mgrn1*$^{m/m}$ embryos treated with no, low (1 nM), or high (25 nM) concentrations of SHH. Each cell line tested was derived from a different embryo. Bars denote the median *Gli1* mRNA values derived from the four individual measurements shown as circles. Statistical significance was determined by one-way ANOVA; not-significant (ns) > 0.05 and ****p-value ≤ 0.0001.

(C) Violin plots with horizontal lines denoting the median and interquartile range summarizing quantification of SMO fluorescence at ~15-50 cilia from pMEFs of the indicated genotypes treated with no SHH or high SHH (25 nM). Statistical significance was determined by the Kruskal-Wallis test; ****p-value ≤ 0.0001.

(**D**) Graph showing the number of digits per limb in embryos of the indicated genotypes treated with Vismodegib. Each circle represents a single limb (forelimb and hindlimb) and the pink lines depict the median with interquartile range. Statistical significance was determined by Kruskal-Wallis; not-significant (ns) > 0.05 and ****p-value ≤ 0.0001.

(**E**) Table summarizing digit number in embryos of various genotypes, with or without Vismodegib treatment according to the regimen shown in Fig. 1C.

(**F**) A model for how the interaction between Vismodegib exposure and genotype influences digit number by altering the strength of Hh signaling.

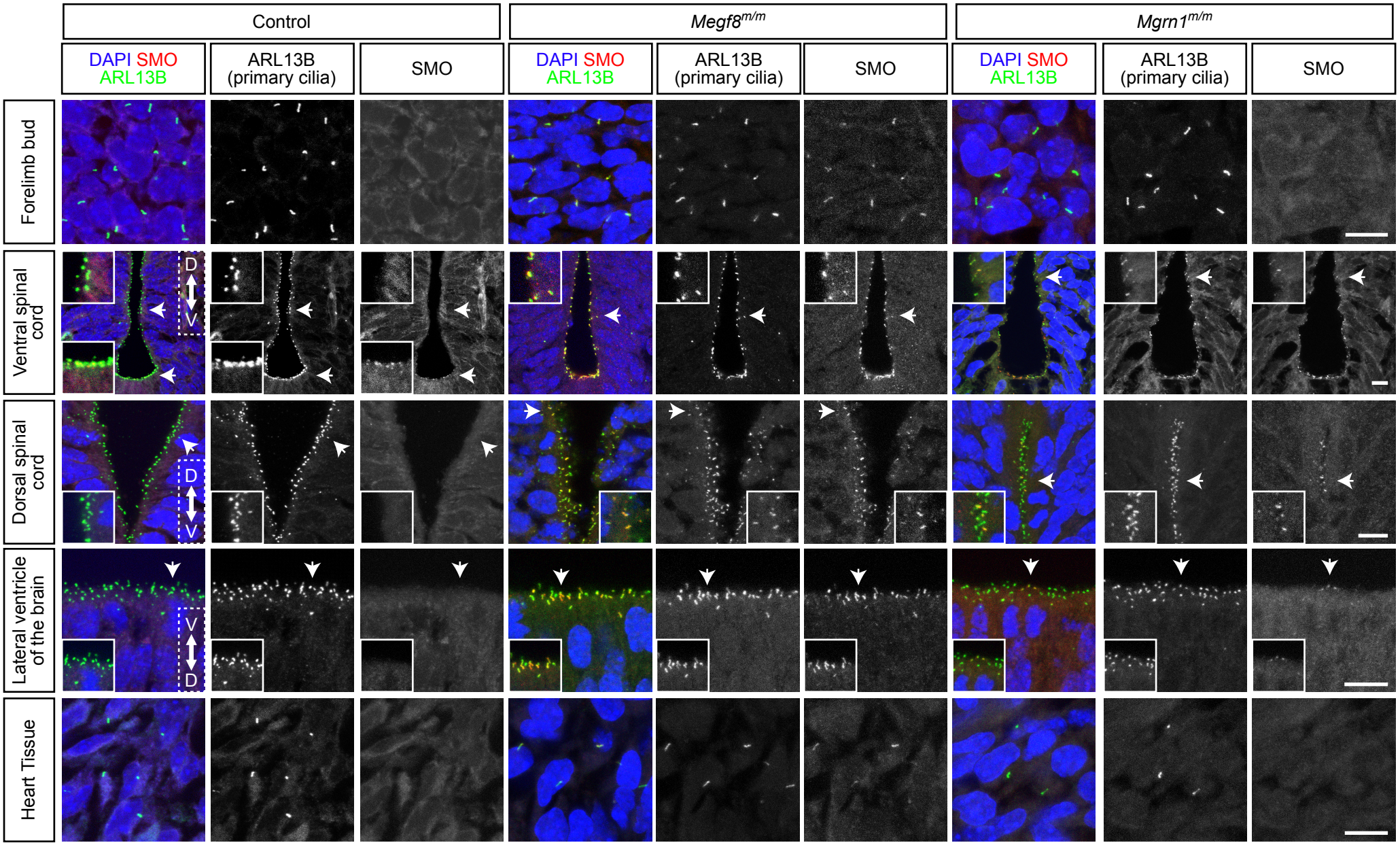
Control
Megf8m/m
Mgrn1m/m
DAPI SMO ARL13B
ARL13B (primary cilia)
SMO
Forelimb bud
Ventral spinal cord
Dorsal spinal cord
Lateral ventricle of the brain
Heart Tissue
D
V

Figure S2. Related to Figure 1: *Megf8*$^{m/m}$ and *Mgrn1*$^{m/m}$ embryos have elevated ciliary Smoothened in multiple tissues.

Confocal fluorescence microscopy images of ciliated tissues (forelimb bud, spinal cord, lateral ventricles of the brain, and heart) collected from e12.5 control (*Mgrn1*$^{m/+}$ or *Megf8*$^{m/+}$), *Megf8*$^{m/m}$, and *Mgrn1*$^{m/m}$ embryos. Arrows denote regions enlarged in insets. In control embryos, ciliary SMO was only present in the floor plate of the ventral spinal cord. In contrast, SMO was detected at cilia in all *Megf8*$^{m/m}$ tissues analyzed. SMO was sparsely detected at cilia in the *Mgrn1*$^{m/m}$ spinal cord and brain. Red, SMO; green, ARL13B (primary cilia); blue, DAPI (nuclei). Scale bars, 10 μm.

Figure S3

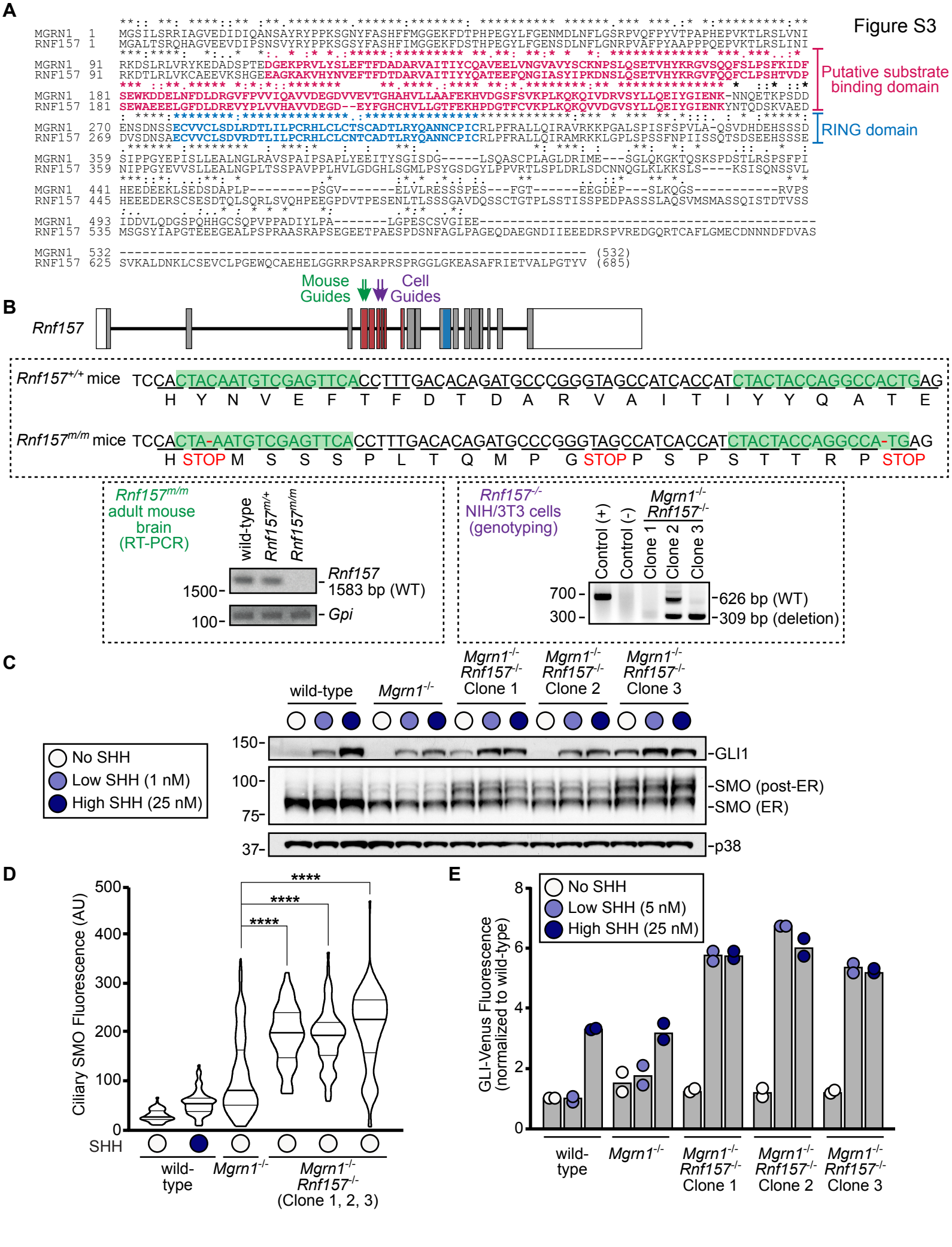
A
MGRN1 1 MGSILSRRIAGVEDIDIQANSAYRYPPKSGNYFASHFFMGGEKFDTPHPEGYLFGENMDLNFLGSRPVQFPYVTPAPHEPVKTLRSLVNI
RNF157 1 MGALTSRQHAGVEEVDIPSNSVYRYPPKSGSYFASHFIMGGEKFDSTHPEGYLFGENSDLNFLGNRPVAFPYAAPPPQEPVKTLRSLINI
MGRN1 91 RKDSLRLVRYKEDADSPTEDGEKPRVLYSLEFTFDADARVAITIYCQAVEELVNGVAVYSCKNPSLQSETVHYKRGVSQQFSLPSFKIDF
RNF157 91 RKDTLRLVKCAEEVKSHGEEAGKAKVHYNVEFTFDTDARVAITIYYQATEEFQNGIASYIPKDNSLQSETVHYKRGVFQQFCLPSHTVDP
MGRN1 181 SEWKDDELNFDLDRGVFPVVIQAVVDEGDVVEVTGHAHVLLAAFEKHVDGSFSVKPLKQKQIVDRVSYLLQEIYGIENK-NNQETKPSDD
RNF157 181 SEWAEEELGFDLDREVYPLVVHAVVDEGD--EYFGHCHVLLGTFEKHPDGTFCVKPLKQKQVVDGVSYLLQEIYGIENKYNTQDSKVAED
MGRN1 270 ENSDNSSECVVCLSDLRDTLILPCRHLCLCTSCADTLRYQANNCPICRLPFRALLQIRAVRKKPGALSPISFSPVLA-QSVDHDEHSSSD
RNF157 269 DVSDNSAECVVCLSDVRDTLILPCRHLCLCNTCADTLRYQANNCPICRLPFRALLQIRAMRKKLGPLSPSSFNPIISSQTSDSEEHSSSE
MGRN1 359 SIPPGYEPISLLEALNGLRAVSPAIPSAPLYEEITYSGISDG-----LSQASCPLAGLDRIME---SGLQKGKTQSKSPDSTLRSPSFPI
RNF157 359 NIPPGYEVVSLLEALNGPLTSSPAVPPLHVLGDGHLSGMLPSYGSDGYLPPVRTLSPLDRLSDCNNQGLKLKKSLS----KSISQNSSVL
MGRN1 441 HEEDEEKLSEDSDAPLP--------PSGV-------ELVLRESSSPES---FGT------EEGDEP---SLKQGS-----------RVPS
RNF157 445 HEEEDERSCSESDTQLSQRLSVQHPEEGPDVTPESENLTLSSSGAVDQSSCTGTPLSSTISSPEDPASSSLAQSVMSMASSQISTDTVSS
MGRN1 493 IDDVLQDGSPQHHGCSQPVPPADIYLPA-------LGPESCSVGIEE----------
RNF157 535 MSGSYIAPGTEEEGEALPSPRAASRAPSEGEETPAESPDSNFAGLPAGEQDAEGNDIIEEEDRSPVREDGQRTCAFLGMECDNNNDFDVAS
MGRN1 532 ---------- (532)
RNF157 625 SVKALDNKLCSEVCLPGEWQCAEHELGGRRPSARPRSPRGGLGKEASAFRIETVALPGTYV (685)
Putative substrate binding domain
RING domain
B
Mouse Guides
Cell Guides
Rnf157
Rnf157+/+ mice TCCACTACAATGTCGAGTTCACCTTTGACACAGATGCCCGGGTAGCCATCACCATCTACTACCAGGCCACTGAG
H Y N V E F T F D T D A R V A I T I Y Y Q A T E
Rnf157m/m mice TCCACTA-AATGTCGAGTTCACCTTTGACACAGATGCCCGGGTAGCCATCACCATCTACTACCAGGCCA-TGAG
H STOP M S S S P L T Q M P G STOP P S P S T T R P STOP
Rnf157m/m adult mouse brain (RT-PCR)
wild-type
Rnf157m/+
Rnf157m/m
1500-
100-
Rnf157 1583 bp (WT)
Gpi
Rnf157-/- NIH/3T3 cells (genotyping)
Mgrn1-/- Rnf157-/-
Control (+)
Control (-)
Clone 1
Clone 2
Clone 3
700-
300-
626 bp (WT)
309 bp (deletion)
C
wild-type
Mgrn1-/-
Mgrn1-/- Rnf157-/- Clone 1
Mgrn1-/- Rnf157-/- Clone 2
Mgrn1-/- Rnf157-/- Clone 3
No SHH
Low SHH (1 nM)
High SHH (25 nM)
150-
100-
75-
37-
GLI1
SMO (post-ER)
SMO (ER)
p38
D
Ciliary SMO Fluorescence (AU)
500
400
300
200
100
0
****
****
****
SHH
wild-type
Mgrn1-/-
Mgrn1-/- Rnf157-/- (Clone 1, 2, 3)
E
GLI-Venus Fluorescence (normalized to wild-type)
8
6
4
2
0
No SHH
Low SHH (5 nM)
High SHH (25 nM)
wild-type
Mgrn1-/-
Mgrn1-/- Rnf157-/- Clone 1
Mgrn1-/- Rnf157-/- Clone 2
Mgrn1-/- Rnf157-/- Clone 3

Figure S3. Related to Figure 2: Loss-of-function mutations in both *Mgrn1* and *Rnf157* results in elevated Hh signaling strength in NIH/3T3 fibroblasts and neural progenitor cells.

(A) Alignment of mouse MGRN1 and RNF157. Red highlights a putative substrate binding domain (Pusapati et al., 2018) unique to proteins related to MGRN1 (tree shown in Fig. 2B), but not found in other RING superfamily E3 ligases. Blue highlights the RING domain. * fully conserved; : strongly similar (scoring > 0.5 in the Gonnet PAM 250 matrix); . weakly similar (scoring ≤ 0.5 in the Gonnet PAM 250 matrix).

(B) CRISPR strategies for targeting *Rnf157* in mice (left, green) and in NIH/3T3 and neural progenitor cells (NPCs) (right, purple). Arrows denote the locations in the genomic map of *Rnf157* targeted by sgRNA guides in mice (green) and cells (purple). Open rectangles denote non-coding exons, gray rectangles denote coding exons, red rectangles denote regions that encode the putative substrate binding domain, blue rectangles denote regions that encode the RING domain, and horizontal lines denote introns. For the generation of *Rnf157*$^{-/-}$ mice, Sanger sequencing was used to identify a 2bp deletion that results in a premature stop codon (sequences are provided in the inset below the exon-intron map). RT-PCR was performed to validate the loss of *Rnf157* expression (bottom left). For the validation of *Rnf157*$^{-/-}$ NIH/3T3 and NPCs, PCR was used to confirm the deletion introduced by co-transfection of two sgRNA guides into the cells (bottom right).

(C and D) Analysis of *Mgrn1*$^{-/-}$;*Rnf157*$^{-/-}$ NIH/3T3 cells. (**C)** Immunoblots showing the abundance of Hh signaling components in extracts of wild-type, *Mgrn1*$^{-/-}$, and three clonal *Mgrn1*$^{-/-}$;*Rnf157*$^{-/-}$ NIH/3T3 cell lines treated with no, low (1 nM), or high (25 nM) concentrations of SHH. (**D**) Violin plots with horizontal lines denoting the median and interquartile range summarize SMO fluorescence in ~40 cilia per sample. Statistical significance was determined by the Kruskal-Wallis test; ****p-value ≤ 0.0001. Clone 3 is featured in the main figures and was used to generate the stable cell lines shown in Fig. 3.

(E) Hh signaling was assessed in NPCs of the indicated genotype exposed to no, low (5 nM), or high (25 nM) concentrations of SHH using a stably integrated fluorescent reporter of target gene induction (GLI-Venus, see (Pusapati et al., 2018)). Bars represent the median GLI-Venus fluorescence (collected from 20,000 cells) from two independent experiments.

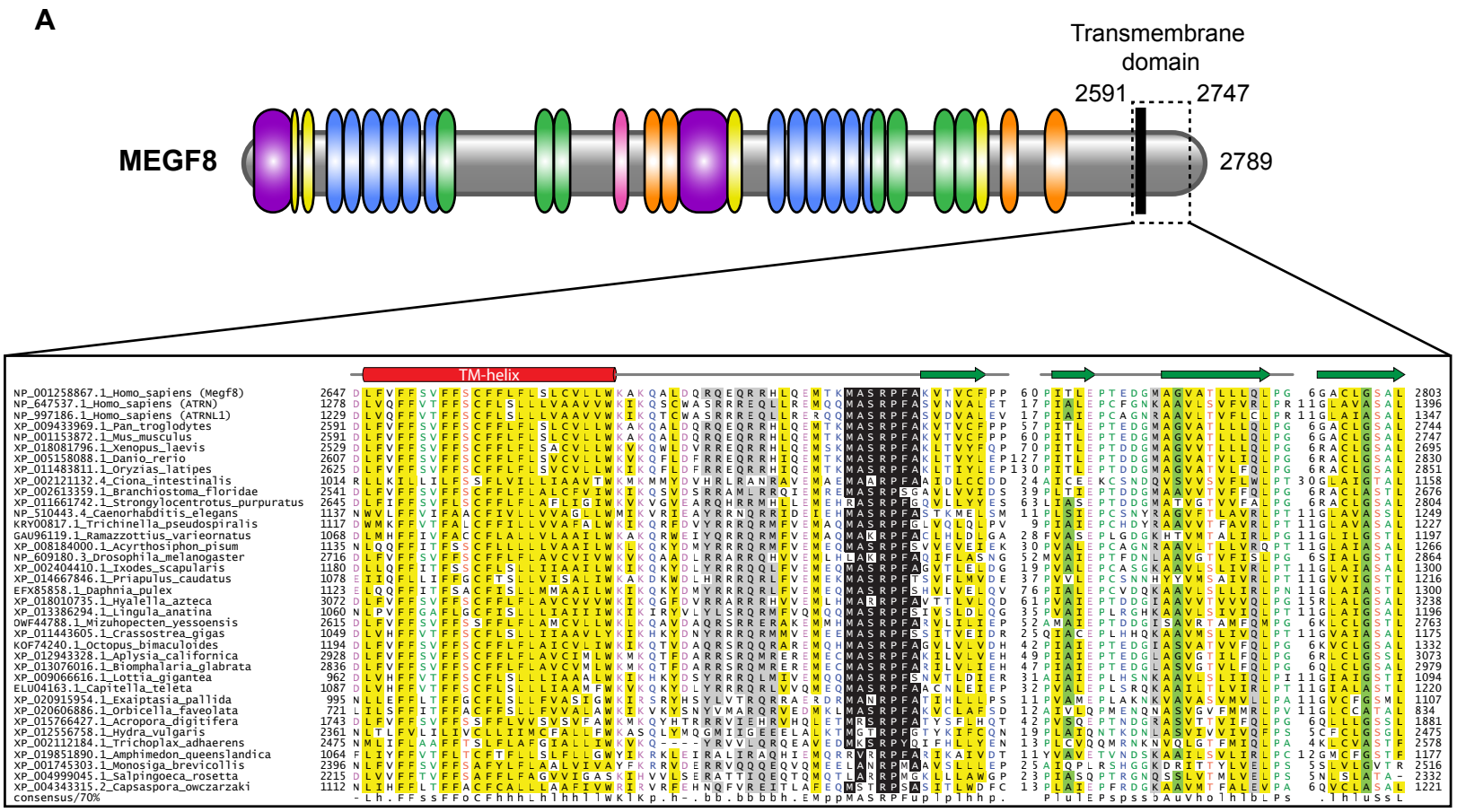
A
Transmembrane domain
2591
2747
MEGF8
2789
TM-helix
NP_001258867.1_Homo_sapiens_(Megf8)
NP_647537.1_Homo_sapiens_(ATRN)
NP_997186.1_Homo_sapiens_(ATRNL1)
XP_009433969.1_Pan_troglodytes
XP_001153872.1_Mus_musculus
XP_018081796.1_Xenopus_laevis
XP_005158088.1_Danio_rerio
XP_011483811.1_Oryzias_latipes
XP_002121132.4_Ciona_intestinalis
XP_002613359.1_Branchiostoma_floridae
XP_011661742.1_Strongylocentrotus_purpuratus
NP_510443.4_Caenorhabditis_elegans
KRY00817.1_Trichinella_pseudospiralis
GAU96119.1_Ramazzottius_varieornatus
XP_008184000.1_Acyrthosiphon_pisum
NP_609180.3_Drosophila_melanogaster
XP_002404410.1_Ixodes_scapularis
XP_014667846.1_Priapulus_caudatus
EFX85858.1_Daphnia_pulex
XP_018010735.1_Hyalella_azteca
XP_013386294.1_Lingula_anatina
OWF44788.1_Mizuhopecten_yessoensis
XP_011443605.1_Crassostrea_gigas
KOF74240.1_Octopus_bimaculoides
XP_012943328.1_Aplysia_californica
XP_013076016.1_Biomphalaria_glabrata
XP_009066616.1_Lottia_gigantea
ELU04163.1_Capitella_teleta
XP_020915954.1_Exaiptasia_pallida
XP_020606886.1_Orbicella_faveolata
XP_015766427.1_Acropora_digitifera
XP_012556758.1_Hydra_vulgaris
XP_002112184.1_Trichoplax_adhaerens
XP_019851890.1_Amphimedon_queenslandica
XP_001745303.1_Monosiga_brevicollis
XP_004999045.1_Salpingoeca_rosetta
XP_004343315.2_Capsaspora_owczarzaki
consensus/70%
B
Putative substrate binding domain
RING domain
278
317
MGRN1
533
1 2 3 4 5 6 7 8 9
Variable Average Conserved
RING mutant #1
C279A/C282A
RING mutant #2
L307A/R308A
Homo sapiens
Pan troglodytes
Mus musculus
Gallus gallus
Xenopus laevis
Callorhinchus milii
Branchiostoma belcheri
Drosophila melanogaster
Caenorhabditis elegans
Daphnia pulex
C
MEGF8 + + + +
MGRN1 − + Mut1 Mut2
Input (3.75%)
IP: MEGF8 (50% Elution)
250-
75-
37-
-MEGF8 (tagged)
-MGRN1
-p38
*

Figure S4. Related to Figure 3: Sequence conservation in selected domains of MGRN1 and MEGF8.

(A) Sequence alignment showing conservation and secondary structure features of the cytoplasmic tail of several members of the MEGF8-ATRN family. The top three proteins are three paralogs (MEGF8, Attractin (ATRN) or Attractin-like (ATRNL1) found in humans and the rest are homologs of these proteins identified in various species. Proteins are named by their GenBank identifiers (GIs), followed by the complete names of the species from which they are derived. Predicted secondary structure elements are shown at the top: the red rectangle denotes a predicted α-helix and the multiple green arrows denote predicted β-strands. Low complexity regions between the strands are hidden and denoted as gaps with numbers. The MASRPFA sequence motif is highlighted in black. The alignment is colored based on 70% consensus with the following scheme as shown in the consensus sequence: h (hydrophobic), l (aliphatic), and a (aromatic) are shaded yellow; p (polar) are shaded blue; charged are shaded pale violet; s (small) and u (tiny) are shaded light green; b (big) is shaded dark gray.

(B) ClustalW alignment of the RING domains of various MGRN1 homologs show conservation of the residues altered to generate the inactive $MGRN1^{Mut1}$ (C279A/C282A) and $MGRN1^{Mut2}$ (L307A/R308A) variants (Gunn et al., 2013). Conservation at each position in the RING domain, color-coded according to the indicated scheme, is based on analysis of 200 homologs of MGRN1 using the ConSurf method (Ashkenazy et al., 2016).

(C) Mutations in the RING domain introduced in $MGRN1^{Mut1}$ and $MGRN1^{Mut2}$ do not abolish their interactions with MEGF8 based on a co-IP experiment after transient expression of the indicated proteins in HEK293T cells (identical to the assay depicted in Fig. 3C). Asterisk (*) indicates endogenous MGRN1 from HEK293T cells that co-precipitated with MEGF8.

Figure S5

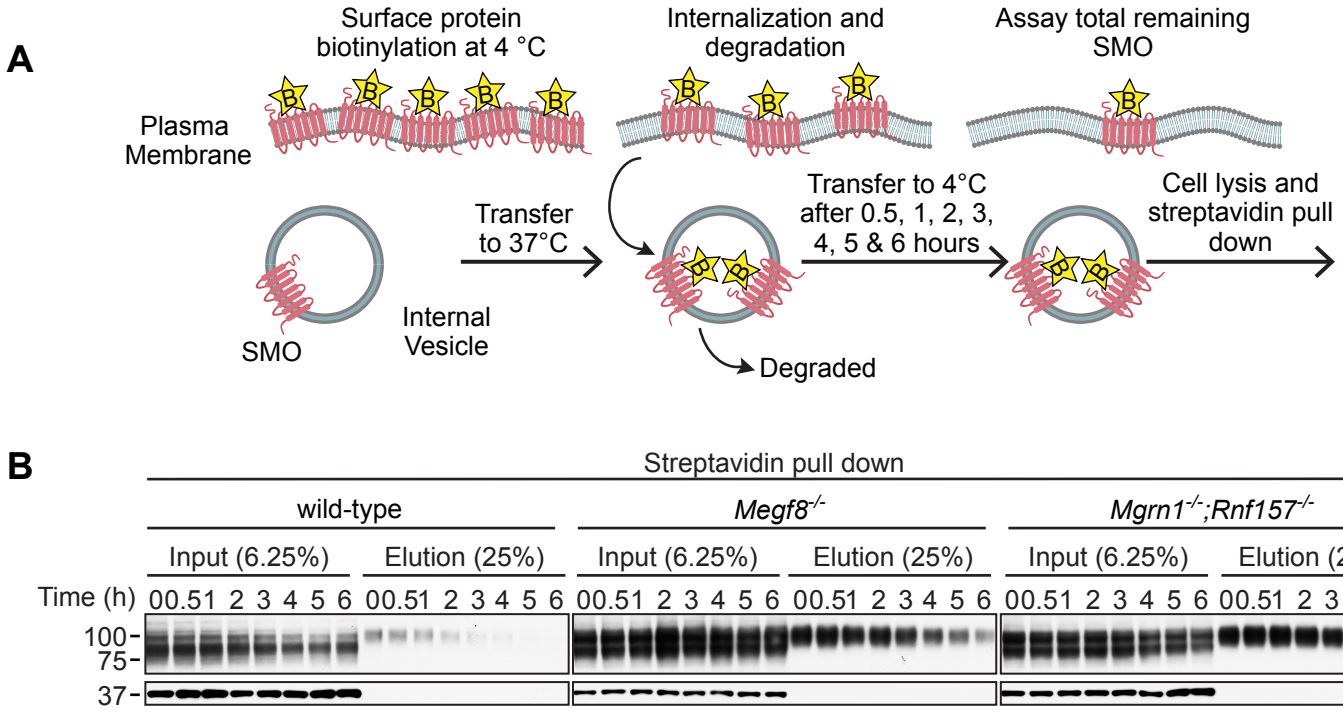
A
Surface protein biotinylation at 4 °C
Internalization and degradation
Assay total remaining SMO
Plasma Membrane
Transfer to 37°C
Transfer to 4°C after 0.5, 1, 2, 3, 4, 5 & 6 hours
Cell lysis and streptavidin pull down
SMO
Internal Vesicle
Degraded
B
Streptavidin pull down
wild-type
Megf8-/-
Mgrn1-/-;Rnf157-/-
Input (6.25%)
Elution (25%)
Time (h)
00.51 2 3 4 5 6
100-
75-
37-
-SMO
-p38

Figure S5. Related to Figure 4: MEGF8 and MGRN1/RNF157 promote the internalization and degradation of SMO at the cell surface.

(A) To measure the degradation rate of cell-surface SMO in wild-type, *Megf8*$^{-/-}$, and *Mgrn1*$^{-/-}$;*Rnf157*$^{-/-}$ NIH/3T3 cells, SMO was labeled with non-cell permeable biotin at 4°C. After warming cells to 37°C to allow for SMO internalization and degradation for various periods of time, the amount of biotinylated SMO remaining was isolated on streptavidin beads and measured by immunoblotting **(B)**. The steady state abundance of SMO (at t=0) was much higher in *Megf8*$^{-/-}$ and *Mgrn1*$^{-/-}$;*Rnf157*$^{-/-}$ cells compared to wild-type cells. The fraction of initial SMO remaining at various times after cell-surface labeling is quantified in and shown in Fig. 4A.

Figure S6

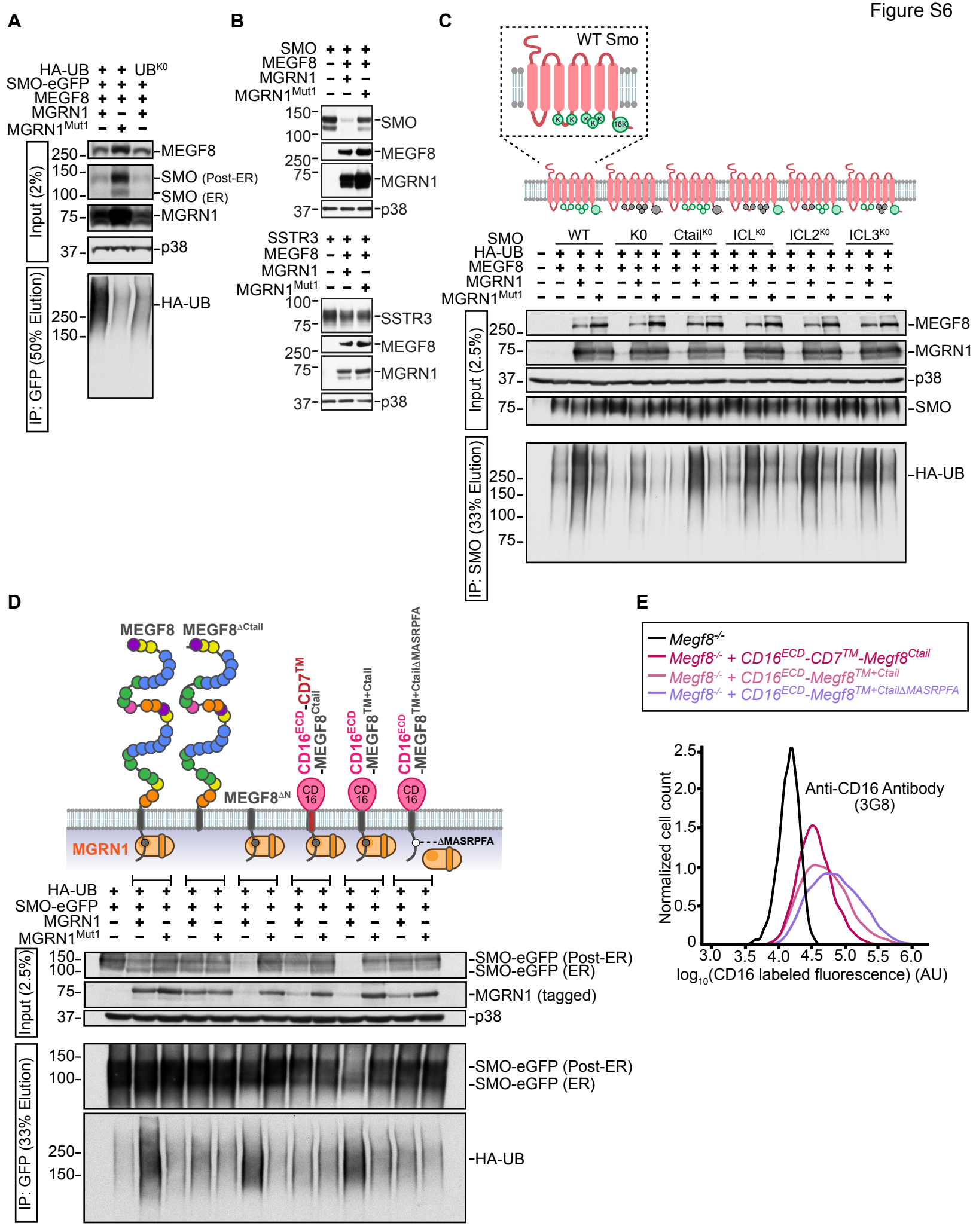
A
HA-UB + + UBK0
SMO-eGFP + + +
MEGF8 + + +
MGRN1 + − +
MGRN1Mut1 − + −
Input (2%)
IP: GFP (50% Elution)
250-
150-
100-
75-
37-
MEGF8
SMO (Post-ER)
SMO (ER)
MGRN1
p38
HA-UB
B
SMO + + +
MEGF8 − + +
MGRN1 − + −
MGRN1Mut1 − − +
SSTR3 + + +
MEGF8 − + +
MGRN1 − + −
MGRN1Mut1 − − +
SMO
MEGF8
MGRN1
p38
SSTR3
C
WT Smo
SMO WT K0 CtailK0 ICLK0 ICL2K0 ICL3K0
HA-UB
MEGF8
MGRN1
MGRN1Mut1
Input (2.5%)
IP: SMO (33% Elution)
MEGF8
MGRN1
p38
SMO
HA-UB
D
MEGF8 MEGF8ΔCtail
CD16ECD-CD7TM-MEGF8Ctail
CD16ECD-MEGF8TM+Ctail
CD16ECD-MEGF8TM+CtailΔMASRPFA
MEGF8ΔN
CD16
MGRN1
ΔMASRPFA
HA-UB
SMO-eGFP
MGRN1
MGRN1Mut1
Input (2.5%)
IP: GFP (33% Elution)
SMO-eGFP (Post-ER)
SMO-eGFP (ER)
MGRN1 (tagged)
p38
HA-UB
E
Megf8-/-
Megf8-/- + CD16ECD-CD7TM-Megf8Ctail
Megf8-/- + CD16ECD-Megf8TM+Ctail
Megf8-/- + CD16ECD-Megf8TM+CtailΔMASRPFA
Anti-CD16 Antibody (3G8)
Normalized cell count
log10(CD16 labeled fluorescence) (AU)

Figure S6. Related to Figure 4: The MEGF8/MGRN1 complex ubiquitinates Smoothened.

(A) Ubiquitination of SMO-eGFP in the presence of wild-type HA-Ubiquitin (HA-UB) or a mutant where all the lysine residues have been mutated to arginine (UB^{K0}) to prevent ubiquitin chain elongation. Ubiquitination was assessed as described in Fig. 4B after transient expression of the indicated proteins in HEK293T cells.

(B) To determine if the MEGF8-MGRN1 complex can regulate the abundance of other G-protein coupled receptors (GPCRs), HEK293T cells were transiently transfected with constructs encoding MEGF8, functional or catalytically inactive MGRN1 ($MGRN1^{Mut1}$), and either SMO (top) or Somatostatin receptor type 3 (SSTR3) (bottom). Immunoblots indicate that co-expression of MEGF8 and MGRN1 complex reduced the abundance of SMO, but had no effect on SSTR3.

(C) Ubiquitination of wild-type SMO or variants carrying mutations in cytoplasmically-exposed lysine residues by the MEGF8-MGRN1 complex. The following five SMO mutants were tested: (1) SMO-K0 (all 21 cytoplasmic lysine residues were changed to arginines), (2) $Smo\text{-}Ctail^{K0}$ (all 16 lysines in the C-terminal cytoplasmic tail were changed to arginines), (3) $SMO\text{-}ICL^{K0}$ (all 5 lysines in the three cytoplasmic loops were changed to arginine), (4) $SMO\text{-}ICL2^{K0}$ (both lysines in the second intracellular loop were changed to arginines), and (5) $SMO\text{-}ICL3^{K0}$ (all three lysines in the third intracellular loop were changed to arginines). Cells were lysed under denaturing conditions, native SMO was purified by IP using beads covalently linked to an anti-SMO antibody, and the amount of HA-UB covalently conjugated to SMO was assessed using immunoblotting with an anti-HA antibody (bottom panel).

(D) Chimeric proteins were used to identify the minimal region of MEGF8 sufficient to support SMO ubiquitination. Using the assay shown in Fig. 4B, SMO ubiquitination was assessed after transient co-expression of the following in 293T cells: SMO-eGFP, HA-UB, MGRN1 (or the inactive mutant $MGRN1^{Mut1}$), and the MEGF8 mutant or chimera shown above the blot. See Fig. 3A and associated text for a description of these chimeras.

(E) Flow cytometry was used to measure cell surface labeled CD16 in live *Megf8*$^{-/-}$ cells stably expressing various CD16/CD7/MEGF8 chimeras (diagrammed in D). These are the same stable cell lines analyzed in Figs. 4D and 4E. 4000 cells were analyzed per condition.

A

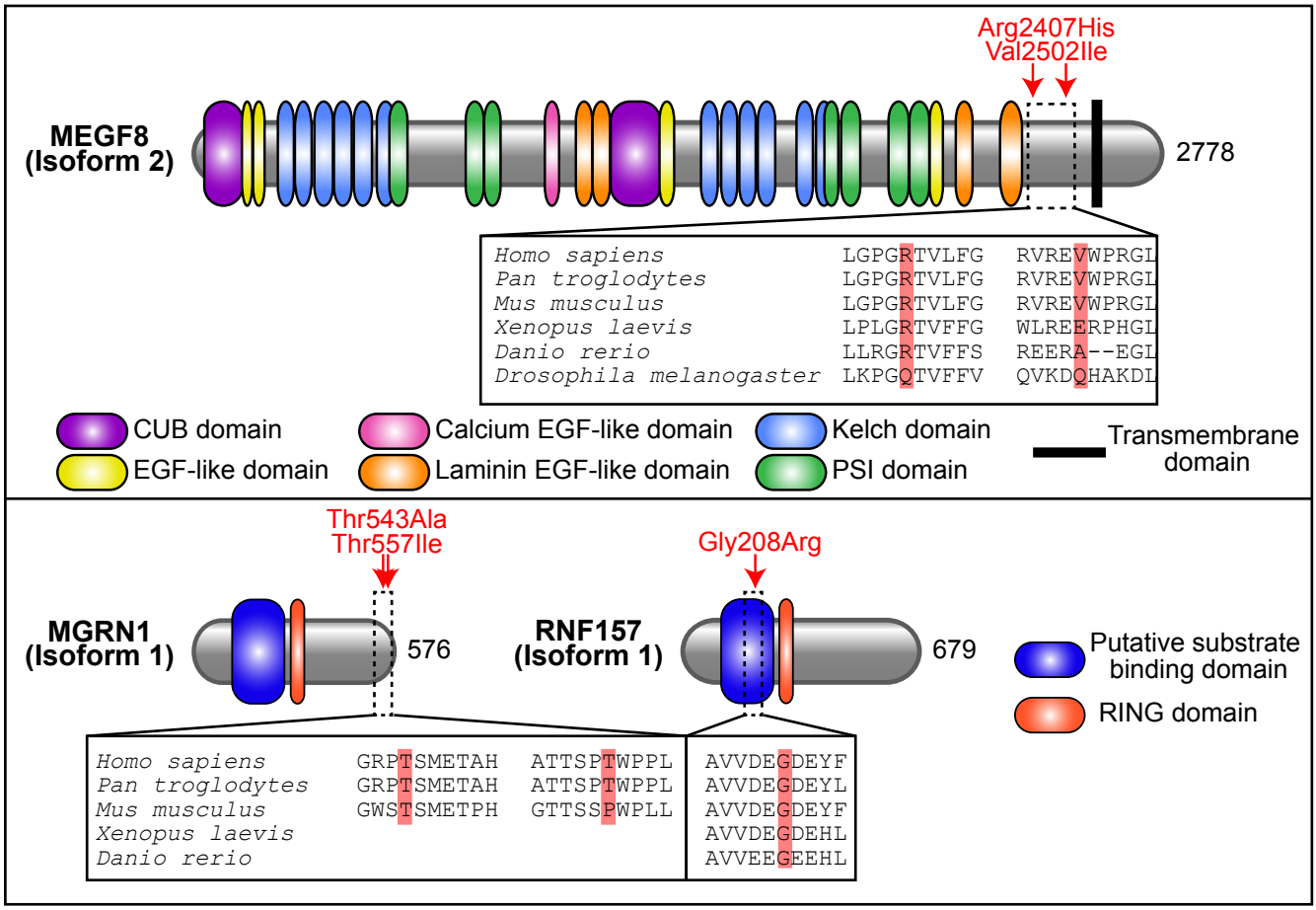

B

	MEGF8		MGRN1		RNF157
Variant	Arg2407His	Val2502Ile	Thr543Ala	Thr557Ile	Gly208Arg
GnomAD AF	0.39%	0.26%	0.014%	0.039%	3.7%
CADD	33.0	14.6	17.1	22.4	34.0
Sift	0 (D)	0.2 (T)	0.38 (T_LC)	0.14 (T_LC)	0 (D)
Polyphen-2	0.997 (D)	0.304 (B)	0.001 (B)	0.206 (B)	0.899 (D)

C

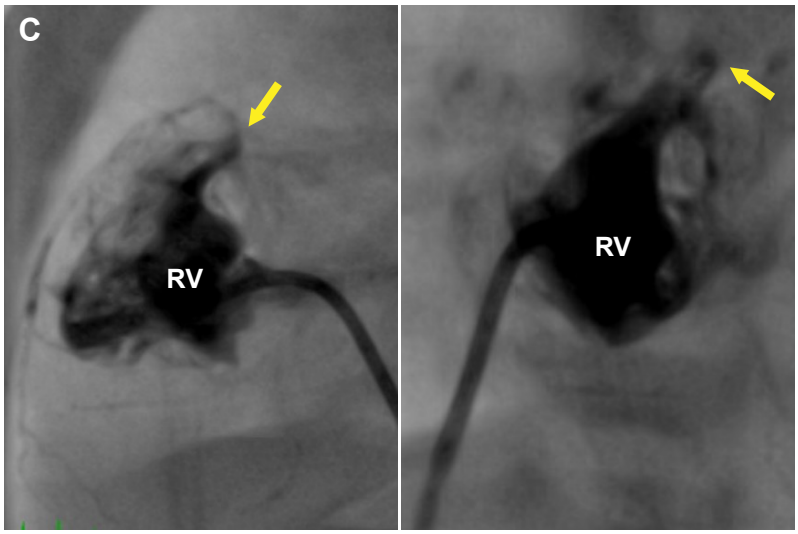

Figure S7. Related to Figure 7: Analysis of human variants in *MEGF8*, *MGRN1*, and *RNF157*.

(A) Schematic representation of the domain composition of human MEGF8, MGRN1, and RNF157 (UniProt Consortium, 2019). Red arrows denote the location of the variants found in patient 7501 (described in Fig. 7A). The conservation of the amino acid residues around the variant of interest is analyzed across model species, with the specific residue altered by the variation shaded in red.

(B) Population allele frequency (AF) of the variants found in patient 7501 is shown from the Genome Aggregation Database (GnomAD). The predicted deleteriousness of each variation on protein structure and function is estimated based on scores from three algorithms: Combined Annotation Dependent Depletion (CADD), Polymorphism Phenotyping v2 (Polyphen-2), or Sorting Intolerant from Tolerant (SIFT). B, benign; D, deleterious; T, tolerated; T_LC, is tolerated (low confidence).

(C) Ventriculogram from patient 7501 in postero-anterior (left) and lateral (right) views demonstrated severely hypoplastic and hypertrophied right ventricle (RV) with an diminutive right ventricular outflow tract. There are copious right ventricular sinusoids coronary fistulas with what is seen of the coronary circulation returning to the aortic root. There was no antegrade flow from the right ventricle to the main pulmonary artery (yellow arrow).

Table S1. Related to Figure 2: Heart, visceral organ situs, and digit number in *Mgrn1*$^{m/m}$, *Rnf157*$^{m/m}$, Megf8$^{m/m}$, and *Mgrn1*$^{m/m}$;*Rnf157*$^{m/m}$ mice.

Rnf157$^{m/m}$ mice

Embryo ID	Body	Heart	VA Alignment	Septal Defect	Aortic Arch	Lung Situs	Abdomen Situs	RF	LF	RH	LH
1	SS	Lev	CC	-	LAA	4R:1L	L(St/Sp/P)	NML	NML	NML	NML
2	SS	Lev	CC	-	LAA	4R:1L	L(St/Sp/P)	NML	NML	NML	NML
3	SS	Lev	CC	-	LAA	4R:1L	L(St/Sp/P)	NML	NML	NML	NML
4	SS	Lev	CC	-	LAA	4R:1L	L(St/Sp/P)	NML	NML	NML	NML
5	SS	Lev	CC	-	LAA	4R:1L	L(St/Sp/P)	NML	NML	NML	NML
6	SS	Lev	CC	-	LAA	4R:1L	L(St/Sp/P)	NML	NML	NML	NML

Mgrn1$^{m/m}$ mice

Embryo ID	Body	Heart	VA Alignment	Septal Defect	Aortic Arch	Lung Situs	Abdomen Situs	RF	LF	RH	LH
1	SIT	Dex	CC	VSD(Ao)	RAA	1R:4L:SIT	R(St/Sp/P)	PDD	PDD	PDD	PDD
2	SS	Lev	CC	-	LAA	4R:1L	L(St/Sp/P)	NML	NML	NML	NML
3	SS	Lev	CC	-	LAA	4R:1L	L(St/Sp/P)	NML	NML	NML	NML
4	SS	Lev	CC	-	LAA	4R:1L	L(St/Sp/P)	NML	NML	NML	NML
5	HTX	Dex	TGA	AVSD	RAA	3R:3L:1M:RPI	L(St/Sp/P)	NML	NML	NML	NML
6	HTX	Dex	TGA	AVSD	RAA	1R:1L:LPI	L(St/Sp/P)	NML	NML	NML	NML
7	SS	Lev	CC	-	LAA	4R:1L	L(St/Sp/P)	NML	NML	NML	NML
8	SS	Lev	CC	-	LAA	4R:1L	L(St/Sp/P)	NML	NML	NML	NML
9	SS	Lev	CC	-	LAA	4R:1L	L(St/Sp/P)	NML	NML	NML	NML
10	SIT	Dex	TGA	AVSD	RAA	1R:4L:SIT	R(St/Sp/P)	NML	NML	NML	NML
11	SS	Lev	CC	-	LAA	4R:1L	L(St/Sp/P)	NML	NML	NML	NML
12	SS	Lev	CC	-	LAA	4R:1L	L(St/Sp/P)	NML	NML	NML	NML
13	SS	Lev	CC	-	LAA	4R:1L	L(St/Sp/P)	NML	NML	NML	NML
14	SS	Lev	CC	-	LAA	4R:1L	L(St/Sp/P)	NML	NML	NML	NML
15	SS	Lev	CC	-	LAA	4R:1L	L(St/Sp/P)	NML	NML	NML	NML

Megf8$^{m/m}$ mice

Embryo ID	Body	Heart	VA Alignment	Septal Defect	Aortic Arch	Lung Situs	Abdomen Situs	RF	LF	RH	LH
1	HTX	Dex	TGA	AVSD	RAA	3R:3L:1M:RPI	L(St/Sp/P)	PDD	PDD	PDD	PDD
2	HTX	Mes	TGA	AVSD	RAA	3R:3L:1M:RPI	R(St/Sp/P)	PDD	PDD	PDD	PDD
3	HTX	Mes	TGA	VSD(Ao)	LAA	3R:3L:1M:RPI	R(St/Sp/P)	N/A	PDD	PDD	PDD
4	HTX	Dex	TGA	AVSD	RAA	1R:1L:LPI	L(St/Sp/P)	PDD	PDD	N/A	PDD
5	HTX	Lev	TGA	AVSD	LAA	3R:3L:1M:RPI	R(St/Sp/P)	PDD	PDD	PDD	PDD
6	HTX	Dex	TGA	-	RAA	3R:3L:1M:RPI	R(St/Sp/P)	PDD	PDD	N/A	PDD
7	HTX	Mes	TGA	AVSD	LAA	3R:3L:1M:RPI	R(St/Sp/P)	PDD	PDD	PDD	PDD
8	HTX	Lev	TGA	AVSD	LAA	3R:3L:1M:RPI	R(St/Sp/P)	PDD	N/A	PDD	PDD
9	HTX	Dex	TGA	-	RAA	3R:3L:1M:RPI	L(St/Sp/P)	PDD	PDD	PDD	PDD
10	HTX	Lev	TGA	AVSD	LAA	3R:3L:1M:RPI	R(St/Sp/P)	PDD	PDD	PDD	PDD
11	HTX	Lev	TGA	AVSD	LAA	4R:1L	R(St/Sp/P)	PDD	PDD	PDD	PDD
12	HTX	Dex	TGA	AVSD	RAA	3R:3L:1M:RPI	L(St/Sp/P)	PDD	PDD	PDD	PDD

Mgrn1$^{m/m}$;*Rnf157*$^{m/m}$ double knockout mice

Embryo ID	Body	Heart	VA Alignment	Septal Defect	Aortic Arch	Lung Situs	Abdomen Situs	RF	LF	RH	LH
1	HTX	Lev	TGA	AVSD	LAA	3R:3L:1M:RPI	L(St/Sp/P)	PDD	PDD	PDD	PDD
2	HTX	Dex	TGA	AVSD	RAA	3R:3L:1M:RPI	L(St/Sp/P)	N/A	PDD	NML	NML
3	HTX	Lev	TGA	AVSD	RAA	3R:3L:1M:RPI	L(St/Sp/P)	PDD	PDD	PDD	PDD

AVSD, atrioventricular septal defect; CC, concordant ventriculoarterial alignment; Dex, dextrocardia; DORV, double outlet right ventricle; HAA, hypoplastic arch; HTA, hypoplastic transverse heart; HTX, heterotaxy; IAA, interrupted aortic arch; LAA, left aortic arch; Lev, levocardia; LF, left forelimb; LH, left hindlimb; LPI, left pulmonary isomerism; L(St/Sp/P), Left sided stomach, spleen, pancreas; Mes, mesocardia; N/A: no digit data collected; NML, normal digit pattern; PDD, preaxial digit duplication; RAA, right aortic arch; RF, right forelimb; RH, right hindlimb; RPI, right pulmonary isomerism; R(St/Sp/P), Right sided stomach, spleen, pancreas; SIT, situs inversus; SS, situs solitus; SymLiv, symmetric liver; TGA, transposition of the great arteries; VA, ventriculoarterial; VSD, ventricular septal defect; VSD(Ao), ventricular septal defect located below the aorta; 1L, one lung lobe on left side; 4R: 4 lung lobes on right side.

Table S2. Related to Figures 5 and 6: Heart, visceral organ situs, and digit number in *Megf8*$^{m/+}$ single heterozygous mice.

Embryo ID	Body	Heart	VA Alignment	Septal Defect	Aortic Arch	Lung Situs	Abdomen Situs	RF	LF	RH	LH
1	SS	Lev	CC	-	LAA	4R:1L	L(St/Sp/P)	NML	NML	NML	N/A
2	SS	Lev	CC	-	LAA	4R:1L	L(St/Sp/P)	N/A	NML	NML	N/A
3	SS	Lev	CC	-	LAA	4R:1L	L(St/Sp/P)	NML	NML	NML	NML
4	SS	Lev	CC	-	LAA	4R:1L	L(St/Sp/P)	N/A	N/A	NML	NML
5	SS	Lev	CC	-	LAA	4R:1L	L(St/Sp/P)	NML	NML	NML	NML
6	SS	Lev	CC	-	LAA	4R:1L	L(St/Sp/P)	NML	NML	NML	NML
7	SS	Lev	CC	-	LAA	4R:1L	L(St/Sp/P)	NML	NML	N/A	N/A
8	SS	Lev	CC	-	LAA	4R:1L	L(St/Sp/P)	NML	NML	N/A	NML
9	SS	Lev	CC	-	LAA	4R:1L	L(St/Sp/P)	NML	NML	NML	NML
10	SS	Lev	CC	-	LAA	4R:1L	L(St/Sp/P)	NML	NML	N/A	NML
11	SS	Lev	CC	-	LAA	4R:1L	L(St/Sp/P)	NML	NML	NML	NML
12	SS	Lev	CC	-	LAA	4R:1L	L(St/Sp/P)	NML	NML	NML	NML
13	SS	Lev	CC	-	LAA	4R:1L	L(St/Sp/P)	NML	NML	NML	NML
14	SS	Lev	CC	-	LAA	4R:1L	L(St/Sp/P)	N/A	NML	NML	NML

CC, concordant ventriculoarterial alignment; LAA, left aortic arch; Lev, levocardia; LF, left forelimb; LH, left hindlimb; L(St/Sp/P), Left sided stomach spleen, pancreas; N/A, no digit data collected; NML, normal digit pattern; RF, right forelimb; RH, right hindlimb; SS, situs solitus,1L, one lung lobe on left side;4R, 4 lung lobes on right side.

Table S3. Related to Figures 5 and 6: Heart, visceral organ situs, and digit number in *Mgrn1*$^{m/+}$ single heterozygous mice.

Embryo ID	Body	Heart	VA Alignment	Septal Defect	Aortic Arch	Lung Situs	Abdomen Situs	RF	LF	RH	LH
1	SS	Lev	CC	-	LAA	4R:1L	L(St/Sp/P)	N/A	NML	NML	N/A
2	SS	Lev	CC	-	LAA	4R:1L	L(St/Sp/P)	NML	NML	NML	NML
3	SS	Lev	CC	-	LAA	4R:1L	L(St/Sp/P)	NML	NML	NML	NML
4	SS	Lev	CC	-	LAA	4R:1L	L(St/Sp/P)	NML	NML	N/A	N/A
5	SS	Lev	CC	-	LAA	4R:1L	L(St/Sp/P)	N/A	N/A	NML	NML
6	SS	Lev	CC	-	LAA	4R:1L	L(St/Sp/P)	NML	NML	NML	NML
7	SS	Lev	CC	-	LAA	4R:1L	L(St/Sp/P)	NML	NML	NML	NML
8	SS	Lev	CC	-	LAA	4R:1L	L(St/Sp/P)	N/A	N/A	N/A	NML
9	SS	Lev	CC	-	LAA	4R:1L	L(St/Sp/P)	NML	NML	NML	NML
10	SS	Lev	CC	-	LAA	4R:1L	L(St/Sp/P)	NML	NML	NML	NML
11	SS	Lev	CC	-	LAA	4R:1L	L(St/Sp/P)	NML	NML	NML	NML
12	SS	Lev	CC	-	LAA	4R:1L	L(St/Sp/P)	N/A	NML	NML	NML
13	SS	Lev	CC	-	LAA	4R:1L	L(St/Sp/P)	NML	NML	N/A	NML
14	SS	Lev	CC	-	LAA	4R:1L	L(St/Sp/P)	NML	NML	N/A	N/A
15	SS	Lev	CC	-	LAA	4R:1L	L(St/Sp/P)	NML	NML	NML	NML

CC, concordant ventriculoarterial alignment; LAA, left aortic arch; Lev, levocardia; LF, left forelimb; LH, left hindlimb; L(St/Sp/P), Left sided stomach spleen, pancreas; N/A, no digit data collected; NML, normal digit pattern; RF, right forelimb; RH, right hindlimb; SS, situs solitus,1L, one lung lobe on left side;4R, 4 lung lobes on right side.

Table S4. Related to Figures 5 and 6: Heart, visceral organ situs, and digit number in *Megf8*$^{m/+}$;*Mgrn1*$^{m/+}$ double heterozygous mice.

Embryo ID	Body	Heart	VA Alignment	Septal Defect	Aortic Arch	Lung Situs	Abdomen Situs	RF	LF	RH	LH
1	SS	Lev	CC	-	LAA	4R:1L	L(St/Sp/P)	PDD	PDD	N/A	N/A
2	SS	Lev	DORV	-	LAA	4R:1L	L(St/Sp/P)	PDD	N/A	N/A	N/A
3	SS	Lev	CC	-	LAA	4R:1L	L(St/Sp/P)	PDD	PDD	N/A	N/A
4	SS	Lev	CC	-	LAA	4R:1L	L(St/Sp/P)	PDD	PDD	PDD	PDD
5	HTX	Dex	CC	-	LAA	4R:1L	L(St/Sp/P)	NML	NML	NA	NML
6	HTX	Lev	DORV	VSD(Ao)	LAA,HAA, IAA	1R:1L:LPI	L(St/Sp/P)	NML	NML	NML	NML
7	SS	Lev	CC	-	LAA	4R:1L	L(St/Sp/P)	NML	NML	NML	NML
8	SS	Lev	CC	-	LAA	4R:1L	L(St/Sp/P)	PD	PDD	N/A	N/A
9	SS	Lev	CC	-	LAA	4R:1L	L(St/Sp/P)	NML	NML	NML	NML
10	SS	Lev	CC	AVSD	LAA	2R:1L:LPI	L(St/Sp/P)	PDD	PDD	N/A	N/A
11	SS	Lev	CC	-	LAA	4R:1L	L(St/Sp/P)	NML	NML	NML	NML
12	HTX	Lev	DORV	-	LAA	1R:1L:LPI	L(St/Sp/P)	PDD	PD	N/A	N/A
13	SIT	Dex	DORV	VSD(Pa)	RAA	4L:1R:SI	R(St/Sp/P) SymLiv	NML	NML	NML	NML
14	SS	Lev	CC	-	LAA	4R:1L	L(St/Sp/P)	PDD	PDD	N/A	N/A
15	SS	Lev	DORV	AVSD	LAA	4R:1L	L(St/Sp/P)	NML	NML	NML	NML
16	HTX	Lev	TGA	AVSD	LAA	3R:3L:1M:RPI	R(St/Sp/P) SymLiv	NML	NML	PDD	NML
17	SS	Lev	CC	-	LAA	4R:1L	L(St/Sp/P)	NML	NML	NML	NML
18	HTX	Lev	DORV	VSD(Pa)	LAA	3R:3L:1M:RPI	L(St/Sp/P)	NML	NML	NML	NML
19	SS	Lev	DORV	VSD(Ao)	LAA,HTA	4R:1L	L(St/Sp/P)	NML	NML	PDD	NML
20	HTX	Lev	TGA	VSD(Pa)	LAA	3R:3L:1M:RPI	L(St/Sp/P)	PDD	PDD	PDD	PDD
21	HTX	Mal	TGA	AVSD	LAA	3R:3L:1M:RPI	L(St/Sp/P)	PDD	PDD	N/A	N/A
22	HTX	Dex	TGA	AVSD	RAA	3R:3L:1M:RPI	R(St/Sp/P) SymLiv	PDD	PDD	PDD	PDD
23	SS	Lev	CC	-	LAA	4R:1L	L(St/Sp/P)	NML	NML	PDD	NML
24	SS	Lev	CC	-	LAA	4R:1L	L(St/Sp/P)	NML	NML	NML	NML
25	SS	Lev	CC	-	LAA	4R:1L	L(St/Sp/P)	NML	NML	NML	NML
26	SS	Lev	CC	-	LAA	4R:1L	L(St/Sp/P)	PDD	PDD	PDD	PDD
27	SS	Lev	CC	-	LAA	4R:1L	L(St/Sp/P)	NML	NML	NML	NML
28	HTX	Dex	TGA	AVSD	RAA	3R:3L:1M:RPI	L(St/Sp/P)	PDD	PDD	PDD	PDD
29	SS	Lev	CC	-	LAA	4R:1L	L(St/Sp/P)	NML	NML	NML	NML
30	HTX	Dex	TGA	AVSD	RAA	3R:3L:1M:RPI	R(St/Sp/P) SymLiv	PDD	PDD	N/A	PDD
31	HTX	Lev	TGA	AVSD	LAA	3R:3L:1M:RPI	R(St/Sp/P) SymLiv	PDD	N/A	PDD	PDD
32	SS	Lev	CC	-	LAA	4R:1L	L(St/Sp/P)	PDD	PDD	PDD	PDD
33	SS	Lev	DORV	-	LAA	4R:1L	L(St/Sp/P)	PDD	PDD	N/A	N/A

AVSD, atrioventricular septal defect; CC, concordant ventriculoarterial alignment; Dex, dextrocardia; DORV, double outlet right ventricle; HAA, hypoplastic arch; HTA, hypoplastic transverse heart; HTX, heterotaxy; IAA, interrupted aortic arch; LAA, left aortic arch; Lev, levocardia; LF, left forelimb; LH, left hindlimb; LPI, left pulmonary isomerism; L(St/Sp/P), Left sided stomach, spleen, pancreas; Mal, malrotated; N/A: no digit data collected; NML, normal digit pattern; PDD, preaxial digit duplication; RAA, right aortic arch; RF, right forelimb; RH, right hindlimb; RPI, right pulmonary isomerism; R(St/Sp/P), Right sided stomach, spleen, pancreas; SIT, situs inversus; SS, situs solitus; SymLiv, symmetric liver; TGA, transposition of the great arteries; VA, ventriculoarterial; VSD, ventricular septal defect; VSD(Ao or Pa), ventricular septal defect located below the aorta or pulmonary artery; 1L, one lung lobe on left side; 4R: 4 lung lobes on right side.

Table S5. Related to Figure 6: Heart, visceral organ situs, and digit number in *Megf8*$^{m/+}$;*Mgrn1*$^{m/m}$ mice.

Embryo ID	Body	Heart	VA Alignment	Septal Defect	Aortic Arch	Lung Situs	Abdomen Situs	RF	LF	RH	LH
1	HTX	Lev	DORV	AVSD	RAA	3R:3L:1M:RPI	L(St/Sp/P)	N/A	PDD	PDD	PDD
2	HTX	Lev	DORV	VSD(Ao)	LAA	3R:3L:1M:RPI	L(St/Sp/P)	PDD	PDD	PDD	PDD
3	SS	Lev	CC	-	LAA	4R:1L	L(St/Sp/P)	PDD	PDD	PDD	PDD
4	SS	Lev	CC	-	LAA	4R:1L	L(St/Sp/P)	NML	NML	NML	NML
5	HTX	Lev	TGA	AVSD	RAA	3R:3L:1M:RPI	L(St/Sp/P)	PDD	PDD	PDD	PDD
6	SIT	Dex	TGA	AVSD	RAA	1R:4L:SIT	R(St/Sp/P)	PDD	PDD	PDD	PDD
7	HTX	Dex	TGA	AVSD	RAA	3R:3L:1M:RPI	L(St/Sp/P)	NML	NML	NML	NML

AVSD, atrioventricular septal defect; CC, concordant ventriculoarterial alignment; Dex, dextrocardia; DORV, double outlet right ventricle; HTX, heterotaxy; LAA, left aortic arch; Lev, levocardia; LF, left forelimb; LH, left hindlimb; L(St/Sp/P), Left sided stomach, spleen, pancreas; N/A: no digit data collected; NML, normal digit pattern; PDD, preaxial digit duplication; RAA, right aortic arch; RF, right forelimb; RH, right hindlimb; RPI, right pulmonary isomerism; SIT, situs inversus; SS, situs solitus; TGA, transposition of the great arteries; VSD, ventricular septal defect; VSD(Ao), ventricular septal defect located below the aorta; 1L, one lung lobe on left side; 4R: 4 lung lobes on right side.

Table S6. Related to Figure 6: Heart, limb, and laterality defects in *Megf8, Mgrn1,* and *Rnf157* mutant mice.

Embryo genotype	CHD	DORV	TGA	AVSD	VSD	Dextrocardia	Heterotaxy	Situs inversus	Preaxial digit duplication
Rnf157$^{m/m}$ n=6	0 (0%)	0 (0%)	0 (0%)	0 (0%)	0 (0%)	0 (0%)	0 (0%)	0 (0%)	0 (0%)
Megf8$^{m/+}$ n=14	0 (0%)	0 (0%)	0 (0%)	0 (0%)	0 (0%)	0 (0%)	0 (0%)	0 (0%)	0 (0%)
Mgrn1$^{m/+}$ n=15	0 (0%)	0 (0%)	0 (0%)	0 (0%)	0 (0%)	0 (0%)	0 (0%)	0 (0%)	0 (0%)
Mgrn1$^{m/m}$ n=15	4 (27%)	0 (0%)	3 (20%)	3 (20%)	1 (7%)	4 (27%)	2 (13%)	2 (13%)	1 (7%)
Megf8$^{m/+}$ *Mgrn1*$^{m/+}$ n=33	17 (52%)	8 (24%)	7 (21%)	8 (24%)	5 (15%)	5 (15%)	11 (33%)	1 (3%)	20 (61%)
Megf8$^{m/+}$ *Mgrn1*$^{m/m}$ n=7	5 (71%)	2 (29%)	3 (43%)	4 (57%)	1 (14%)	2 (29%)	4 (57%)	1 (14%)	5 (71%)
Megf8$^{m/m}$ n=12	12 (100%)	0 (0%)	12 (100%)	9 (75%)	1 (8%)	5 (42%)	12 (100%)	0 (0%)	12 (100%)
Mgrn1$^{m/m}$ *Rnf157*$^{m/m}$ n=3	3 (100%)	0 (0%)	3 (100%)	3 (100%)	0 (0%)	1 (33%)	3 (100%)	0 (0%)	3 (100%)

AVSD, atrioventricular septal defect; DORV, double outlet right ventricle; CHD, congenital heart defect; TGA, transposition of the great arteries; VSD, ventricular septal defect

Table S7. Related to Figure 6: Laterality of CHD lesions in *Megf8*$^{m/+}$;*Mgrn1*$^{m/+}$ double heterozygous mice.

Specific CHD	Situs Solitus	Situs Inversus	Heterotaxy
DORV n=8	4 (50%)	1 (12.5%)	3 (37.5%)
TGA n=7	0 (0%)	0 (0%)	7 (100%)
AVSD n=8	2 (25%)	0 (0%)	6 (75%)
VSD n=5	1 (20%)	1 (20%)	3 (60%)

AVSD, atrioventricular septal defect; DORV, double outlet right ventricle; TGA, transposition of the great arteries; VSD, ventricular septal defect

Table S8. Related to Figure 7: Whole exome sequencing of patient 7501.

Sample ID	Gene	Chr:Position	Ref	Alt	Ref SNP	CADD PHREDD	GenomAD AF	Variant
7501	MGRN1	16:4738805	A	G	rs369718932	17.14	0.01377%	c.1627A>G:p.Thr543Ala
7501	MGRN1	16:4738848	C	T	rs200375426	22.4	0.03913%	c.1670C>T:p.Thr557Ille
7501	RNF157	17:74162548	C	T	rs11539879	34	3.695%	c.622G>A:p.Gly208Arg
7501	MEGF8	19:42879810	G	A	rs45623135	33	0.3952%	c.7220G>A:p.Arg2407His
7501	MEGF8	19:42880094	G	A	rs147133204	14.57	0.2581%	c.7504G>A:p.Val2502Ile

Table S9. Related to STAR Methods Key Resource Table: Oligonucleotides

REAGENT or RESOURCE	SOURCE	IDENTIFIER
Oligonucleotides		
mGli1 qRT-PCR Primer, Fwd: 5'-CCAAGCCAACTTTATGTCAGGG-3'	Pusapati et al., 2018	N/A
mGli1 qRT-PCR Primer, Rev: 5'-AGCCCGCTTCTTTGTTAATTTGA-3'	Pusapati et al., 2018	N/A
mGapdh qRT-PCR Primer, Fwd: 5'-AGTGGCAAAGTGGAGATT-3'	Pusapati et al., 2018	N/A
mGapdh qRT-PCR Primer, Rev: 5'-GTGGAGTCATACTGGAACA-3'	Pusapati et al., 2018	N/A
hGLI1 qRT-PCR Primer, Fwd: 5'-CAGGGAGGAAAGCAGACTGA-3'	This paper	N/A
hGLI1 qRT-PCR Primer, Rev: 5'-ACTGCTGCAGGATGACTGG-3'	This paper	N/A
hGAPDH qRT-PCR Primer, Fwd: 5'-GTCTCCTCTGACTTCAACAGCG-3'	This paper	N/A
hGAPDH qRT-PCR Primer, Rev: 5'-ACCACCCTGTTGCTGTAGCCAA-3'	This paper	N/A
mRnf157 qRT-PCR Primer (mice) Fwd: 5'-ATCCCGTCCAATTCCGTGTA-3'	This paper	N/A
mRnf157 qRT-PCR Primer (mice) Rev: 5'-GTACCAGGTGCGATGTAGGA-3'	This paper	N/A
*mGpi q*RT-PCR Primer (mice) Fwd: 5'-CAACTGCTACGGCTGTGAGA-3'	Gunn et al., 2013	N/A
mGpi qRT-PCR Primer (mice) Rev: 5'- CTTTCCGTTGGACTCCATGT-3'	Gunn et al., 2013	N/A
mRnf157 genotyping PCR Primer (cells), Fwd: 5'-GAGCAGAGAGGAGGTTAGCG-3'	This paper	N/A
mRnf157 genotyping PCR Primer (cells), Rev: 5'-CAAGCTAGACCTTCCCGAGG-3'	This paper	N/A
mRnf157 genotyping wild-type PCR Primer (mice), Fwd: 5'-AGGCAAAGCTAAGGTCCACTAC-3'	This paper	N/A
mRnf157 genotyping mutant PCR Primer (mice), Fwd: 5'-AGGCAAAGCTAAGGTCCACTAA-3'	This paper	N/A
mRnf157 genotyping common PCR Primer (mice), Rev: 5'-CCTGCTATGCCGTCTTACCT-3'	This paper	N/A
mRnf157 sgRNA target sequence PCR Primer (mice), Fwd: 5'-AACAAAGTCCCGATCCACTG-3'	This paper	N/A
mRnf157 sgRNA target sequence PCR Primer (mice), Rev1: 5'-CAAGCTAGACCTTCCCGAGG-3'	This paper	N/A
mRnf157 sgRNA target sequence PCR Primer (mice), Rev2: 5'-CCTTTCAGCATGGCTTTCTC-3'	This paper	N/A
Mgrn1$^{md\text{-}nc}$ genotyping wild-type PCR primer, Fwd: 5'-GCCTGCATGGATAGATGGAT-3'	Gunn et al., 2019	N/A
Mgrn1$^{md\text{-}nc}$ genotyping wild-type PCR primer Rev: 5'-AGGAAGTTGCCCACAAGAACGCA-3'	Gunn et al., 2019	N/A
Mgrn1$^{md\text{-}nc}$ genotyping mutant PCR primer, Fwd: 5'-CAAGAACAACCAGGAGACTAAGGA-3'	Gunn et al., 2019	N/A
Mgrn1$^{md\text{-}nc}$ genotyping mutant PCR primer, Rev: 5'-GCCCAAGTCCTAAACCTCT-3'	Gunn et al., 2019	N/A
Megf8^{C193R} genotyping PCR Primer Set 1, Fwd: 5'-ACGACCCATATCTCTGCCTT-3'	This paper	N/A
Megf8^{C193R} genotyping PCR Primer Set 1, Rev: 5'-GCCTCCAGACCCTCCAAG-3'	This paper	N/A
Megf8^{C193R} genotyping common PCR Primer Set 2, Fwd: 5'-CTCAGCTCTGCACCCCTAAC-3'	This paper	N/A
Megf8^{C193R} genotyping wild-type PCR Primer Set 2, Rev: 5'-TCCCAAGAATCCAGGTTCACA-3'	This paper	N/A
Megf8^{C193R} genotyping mutant PCR Primer Set 2, Rev: 5'-CCAAGAATCCAGGTTCACG-3'	This paper	N/A

File S1. Related to Figure 2: Newick tree file for the MGRN1-RNF157 family.

(MGRN1_XP_626702.1_Cryptosporidium_parvum:6.4556799939,((((MGRN1_XP_012750170.1_Acytostelium_subglobosum:0.8834035749,MGRN1_EFA84789.1_Heterostelium_album:0.7564698726)100:1.0990476127,MGRN1_XP_646206.1_Dictyostelium_discoideum:1.9725849426)100:3.1996779932,((((((((((((MGRN1_XP_022252119.1_Limulus_polyphemus:0.7130424361,MGRN1_XP_002434259.1_Ixodes_scapularis:0.8067633411)100:0.3546045995,(((MGRN1_XP_021208538.1_Bombyx_mori:0.0000022207,MGRN1_XP_012551644.1_Bombyx_mori:0.0000022207)100:0.6674373775,(MGRN1_XP_008197724.1_Tribolium_castaneum:0.6043109157,((MGRN1_XP_624563.2_Apis_mellifera:0.0000022207,MGRN1_XP_006571957.1_Apis_mellifera:0.0000022207)100:0.0978541753,MGRN1_XP_011144180.1_Harpegnathos_saltator:0.1639699560)100:0.4188667910)100:0.1383218127)97:0.1390462809,(MGRN1_NP_572915.1_Drosophila_melanogaster:0.7240618615,MGRN1_XP_001842757.1_Culex_quinquefasciatus:0.4930549513)100:0.5592043648)98:0.1659530383)99:0.1601768095,MGRN1_XP_003378072.1_Trichinella_spiralis:2.4613076368)96:0.1652080042,MGRN1_OWA53600.1_Hypsibius_dujardini:1.8845700706)100:0.3022685831,((((MGRN1_XP_009012902.1_Helobdella_robusta:1.4199350327,MGRN1_XP_011456291.1_Crassostrea_gigas:0.9744293918)68:0.1827551179,MGRN1_XP_013395504.1_Lingula_anatina:0.9435380355)68:0.1936942442,MGRN1_XP_014772328.1_Octopus_bimaculoides:0.8240707803)77:0.2250694468,MGRN1_XP_009056095.1_Lottia_gigantea:0.9606406571)100:0.3497208259)98:0.2460667652,((((MGRN1_XP_015752852.1_Acropora_digitifera:1.8098585308,MGRN1_KXJ08562.1_Exaiptasia_pallida:0.2865159553)100:0.8920209580,MGRN1_XP_001630091.1_Nematostella_vectensis:0.6942822428)100:1.1606397688,(MGRN1_XP_002109227.1_Trichoplax_adhaerens:2.2929217319,MGRN1_XP_012558349.1_Hydra_vulgaris:2.6718292265)95:0.4159482970)94:0.2982637166,MGRN1_XP_018671577.1_Ciona_intestinalis:2.4449979012)45:0.1600650448)40:0.1743552262,(MGRN1_XP_011681930.1_Strongylocentrotus_purpuratus:1.2412630478,MGRN1_XP_006816719.1_Saccoglossus_kowalevskii:0.6956647937)100:0.3512516240)39:0.1272151383,MGRN1_XP_002607160.1_Branchiostoma_floridae:1.5874372991)86:0.4011963809,((((MGRN1_NP_001138254.1_Danio_rerio:0.1542059135,MGRN1_CAG12208.1_Tetraodon_nigroviridis:0.0900101225)100:0.0965540188,MGRN1_XP_017339726.1_Ictalurus_punctatus:0.5529251973)100:0.1053269429,(MGRN1_XP_018096102.1_Xenopus_laevis:0.6339067055,(((MGRN1_XP_006521895.1_Mus_musculus:0.0881653705,MGRN1_ELK34685.1_Myotis_davidii:0.2355299819)99:0.0271033339,MGRN1_NP_056061.1_Homo_sapiens:0.1092290169)100:0.1239586071,MGRN1_XP_004945431.2_Gallus_gallus:0.1734568780)99:0.0546549251)98:0.0676536127)100:0.7446594670,((((((((((RNF157_XP_019794160.1_Tursiops_truncatus:0.0715318657,(RNF157_XP_007454376.1_Lipotes_vexillifer:0.0078127635,RNF157_XP_012390593.1_Orcinus_orca:0.0417563415)100:0.0039693380)100:0.0274949628,RNF157_OWK14388.1_Cervus_elaphus:0.0343731679)96:0.0138497635,(((RNF157_XP_014387228.1_Myotis_brandtii:0.5339584241,(RNF157_XP_015982952.1_Rousettus_aegyptiacus:0.0641276630,(RNF157_ELK12342.1_Pteropus_alecto:0.0021467044,RNF157_XP_011360372.1_Pteropus_vampyrus:0.2733353942)99:0.0222111173)99:0.0432625583)100:0.0410727678,((((RNF157_XP_006107235.1_Myotis_lucifugus:0.0209344513,RNF157_XP_015414699.1_Myotis_davidii:0.0757533803)100:0.0969409524,RNF157_XP_013845346.1_Sus_scrofa:0.1680616436)88:0.0743225206,(RNF157_XP_004655748.1_Jaculus_jaculus:0.0764856949,RNF157_XP_005624217.1_Canis_lupus:0.0583989552)87:0.0142601111)80

:0.0116044543,(RNF157_XP_017529823.1_Manis_javanica:0.0678685327,(RNF157_XP_0075
36806.1_Erinaceus_europaeus:0.0259028420,(RNF157_XP_012588480.1_Condylura_cristata:
0.0883633390,RNF157_XP_012789771.1_Sorex_araneus:0.1336762544)100:0.0135134547)9
9:0.0082482797)96:0.0098075317)79:0.0075837417)68:0.0120886129,RNF157_EQB77236.1_
Camelus_ferus:0.2062033966)93:0.0215268641)97:0.0053043244,RNF157_XP_019500002.1_
Hipposideros_armiger:0.0425196353)98:0.0082871101,((((RNF157_XP_017391079.1_Cebus_
capucinus:0.0635807445,((RNF157_AAH04231.2_Homo_sapiens:0.3429153408,RNF157_NP_
443148.1_Homo_sapiens:0.0039774845)99:0.0153998507,(RNF157_XP_017740235.1_Rhinop
ithecus_bieti:0.0389188257,RNF157_XP_008009863.1_Chlorocebus_sabaeus:0.0699256935)
100:0.0043091587)99:0.0019014587)99:0.0106880921,RNF157_XP_012658433.1_Otolemur_
garnettii:0.0626974246)100:0.0035982813,(RNF157_NP_081534.1_Mus_musculus:0.0648491
574,RNF157_XP_004592943.1_Ochotona_princeps:0.0864653650)99:0.0049199899)100:0.00
77707120,RNF157_XP_004374441.1_Trichechus_manatus:0.0820793497)95:0.0036907473)9
9:0.0419720673,RNF157_XP_016083403.1_Ornithorhynchus_anatinus:0.3883801346)93:0.01
21062608,RNF157_XP_003768510.1_Sarcophilus_harrisii:0.0747707403)100:0.0664719130,((
((RNF157_XP_014435712.1_Pelodiscus_sinensis:0.0847040242,RNF157_XP_008162104.1_C
hrysemys_picta:0.3616339896)95:0.0326348156,RNF157_XP_006018423.2_Alligator_sinensis
:0.0482559786)91:0.0347732273,((RNF157_XP_009664550.1_Struthio_camelus:0.057139492
2,RNF157_XP_013797312.1_Apteryx_mantelli:0.0629791352)98:0.0332317156,((RNF157_XP
_010299131.1_Balearica_regulorum:0.5279873468,((((RNF157_XP_009914760.1_Haliaeetus_
albicilla:0.1297778575,(((RNF157_XP_021270628.1_Numida_meleagris:0.0158663718,RNF15
7_XP_015150798.1_Gallus_gallus:0.0100129247)100:0.0838907874,RNF157_XP_009562266.
1_Cuculus_canorus:0.0499423928)98:0.0155239002,RNF157_XP_009636045.1_Egretta_garz
etta:0.1132778761)58:0.0000026051)92:0.0139762340,RNF157_XP_010142984.1_Buceros_rh
inoceros:0.0399010091)78:0.0084636664,((((RNF157_XP_012433989.1_Taeniopygia_guttata:
0.3336668594,RNF157_XP_021397362.1_Lonchura_striata:0.0317956558)99:0.0088702849,R
NF157_XP_016158280.1_Ficedula_albicollis:0.0848070169)87:0.0126059415,(RNF157_XP_0
14127545.1_Zonotrichia_albicollis:0.0996621112,(RNF157_XP_019146210.1_Corvus_cornix:0.
0388465764,RNF157_XP_017688572.1_Lepidothrix_coronata:0.0346467421)90:0.0117236358
)87:0.0282220494)92:0.0187083207,(RNF157_KQK80228.1_Amazona_aestiva:0.0459980143,
RNF157_XP_012983257.1_Melopsittacus_undulatus:0.1876689248)100:0.0931602731)85:0.0
182830049)51:0.0000024413,RNF157_XP_019327654.1_Aptenodytes_forsteri:0.1300043743)
72:0.0133699745)74:0.0096468713,(RNF157_XP_008498014.1_Calypte_anna:0.1579187411,
RNF157_XP_010193349.1_Mesitornis_unicolor:0.0531898268)56:0.0085821787)99:0.1064356
370)100:0.0904064361)57:0.0126676955,(RNF157_XP_016846820.1_Anolis_carolinensis:0.07
43760823,(RNF157_ETE73233.1_Ophiophagus_hannah:0.1534674086,RNF157_XP_0152699
26.1_Gekko_japonicus:0.1622902018)57:0.0190621432)100:0.0680287271)100:0.0513493674
)100:0.0602604858,(RNF157_XP_018092914.1_Xenopus_laevis:0.1062829246,RNF157_XP_
018410793.1_Nanorana_parkeri:0.0548212369)100:0.3383893646)99:0.1080653267,RNF157_
XP_014342274.1_Latimeria_chalumnae:0.2320355122)96:0.0467261359,(((((((RNF157_XP_0
05952432.2_Haplochromis_burtoni:0.2853462810,(RNF157_XP_008294193.1_Stegastes_parti
tus:0.0070064422,((RNF157_XP_020792200.1_Boleophthalmus_pectinirostris:0.2404359276,R
NF157_XP_015818331.1_Nothobranchius_furzeri:0.0611955329)98:0.0185998689,RNF157_X
P_018521135.1_Lates_calcarifer:0.0122103587)85:0.0057484926)80:0.0000024663)93:0.0101

518814,RNF157_XP_003978203.2_Takifugu_rubripes:0.0825142682)100:0.0711936727,((RNF157_XP_021436693.1_Oncorhynchus_mykiss:0.0265075529,RNF157_XP_014068740.1_Salmo_salar:0.0279331129)100:0.1176562479,RNF157_XP_012987491.1_Esox_lucius:0.0784892020)100:0.0647841386)100:0.0741729306,RNF157_XP_012691288.1_Clupea_harengus:0.2435050180)99:0.0160095459,((RNF157_XP_017558155.1_Pygocentrus_nattereri:0.0285236736,RNF157_XP_017338147.1_Ictalurus_punctatus:0.1652275577)100:0.0864146530,RNF157_XP_018963967.1_Cyprinus_carpio:0.0972291116)99:0.0462892325)99:0.0428323245,RNF157_XP_018617615.1_Scleropages_formosus:0.0990364186)94:0.0435787077,RNF157_XP_015211982.1_Lepisosteus_oculatus:0.1570006008)100:0.2679641271,(RNF157_XP_007884001.1_Callorhinchus_milii:0.3257010038,RNF157_XP_020381796.1_Rhincodon_typus:0.5614613586)97:0.1285779675)93:0.0265497081)100:0.6580846945)100:0.4900158004)99:0.4651716473,MGRN1_XP_019849223.1_Amphimedon_queenslandica:3.6035969064)62:0.1807345037,((MGRN1_CBY07841.1_Oikopleura_dioica:2.7847834568,MGRN1_OAF67975.1_Intoshia_linei:4.0678441542)84:0.7054571260,(MGRN1_NP_510385.1_Caenorhabditis_elegans:1.5469957734,(MGRN1_XP_001892209.1_Brugia_malayi:0.5608706112,MGRN1_ERG87446.1_Ascaris_suum:0.6510690897)100:1.0134141185)100:1.1752088817)56:0.4547444207)95:0.6156688389,((((MGRN1_XP_004346075.1_Capsaspora_owczarzaki:1.2611631116,MGRN1_XP_014158540.1_Sphaeroforma_arctica:3.5625632456)98:0.8367261412,MGRN1_XP_004992715.1_Salpingoeca_rosetta:2.2705221465)94:1.1062203011,(MGRN1_XP_013760930.1_Thecamonas_trahens:4.6514487514,MGRN1_XP_009496900.1_Fonticula_alba:7.1644480376)70:2.3964454855)58:0.7467699989,(((MGRN1_ORX91900.1_Basidiobolus_meristosporus:2.5042194473,(MGRN1_KNE56649.1_Allomyces_macrogynus:2.1174716183,MGRN1_ORZ33642.1_Catenaria_anguillulae:2.1224826073)100:3.6582738324)100:0.8564694622,MGRN1_KFH67492.1_Mortierella_verticillata:3.1705019833)100:1.5530686992,(MGRN1_XP_006675586.1_Batrachochytrium_dendrobatidis:3.3171805662,MGRN1_XP_016604932.1_Spizellomyces_punctatus:2.6740192696)100:1.7578620674)96:0.8431626334)61:0.4916394823)87:0.4672283754,((((((MGRN1_XP_005786359.1_Emiliania_huxleyi:2.7875210880,MGRN1_XP_005819899.1_Guillardia_theta:1.8657262631)99:1.0565410313,(((((MGRN1_XP_011396820.1_Auxenochlorella_protothecoides:1.4193882969,MGRN1_XP_005849270.1_Chlorella_variabilis:0.7250397887)100:0.3787123806,MGRN1_XP_005648141.1_Coccomyxa_subellipsoidea:0.9471512839)100:1.1869157110,MGRN1_XP_001703291.1_Chlamydomonas_reinhardtii:1.7371911370)100:0.7223991659,((MGRN1_XP_002508870.1_Micromonas_commoda:1.3760598152,MGRN1_XP_003063967.1_Micromonas_pusilla:1.5889584546)100:0.5886215128,MGRN1_XP_003083824.1_Ostreococcus_tauri:3.5681305083)100:0.8763305688)99:0.4492440239,(((((MGRN1_XP_015159045.1_Solanum_tuberosum:0.9988391110,MGRN1_NP_566356.1_Arabidopsis_thaliana:0.8353173904)100:0.4039170893,MGRN1_NP_001333932.1_Zea_mays:0.6619418321)100:0.8913461077,(MGRN1_XP_016464410.1_Nicotiana_tabacum:0.6756830166,MGRN1_XP_010659828.1_Vitis_vinifera:0.7763921462)100:1.4485243926)99:0.2272140046,(MGRN1_XP_001764144.1_Physcomitrella_patens:1.1831346121,MGRN1_XP_002982812.1_Selaginella_moellendorffii:0.9015411581)83:0.2312402188)100:0.8165187923,MGRN1_GAQ89054.1_Klebsormidium_nitens:1.6139073283)100:0.4675215425)99:0.9331956584)94:0.4040903123,(((MGRN1_XP_012193830.1_Saprolegnia_parasitica:0.1115517198,MGRN1_XP_008607414.1_Saprolegnia_diclina:0.0641701944)100:0.7326918078,MGRN1_XP_009843084.1_Aphanomyces_astaci:1.2869041723)100:1.1833250169,MGRN1_XP_009529847.1_Phytophthora_sojae:1.2771853540)100:2.7188904758)88:0.558

2954625,(((MGRN1_XP_001612895.1_Plasmodium_vivax:3.4315460842,MGRN1_CEM20353.1_Vitrella_brassicaformis:1.3890543205)100:0.6916400651,(MGRN1_XP_003880832.1_Neospora_caninum:0.2718422860,(MGRN1_XP_002368812.1_Toxoplasma_gondii:0.0167429888,MGRN1_XP_008887669.1_Hammondia_hammondi:0.0637855327)80:0.1327641691)99:1.7622695251)99:1.1437754151,MGRN1_XP_002769107.1_Perkinsus_marinus:4.1019957488)99:1.6755472339)76:0.4117119488,MGRN1_EWM25530.1_Nannochloropsis_gaditana:4.8947789704)62:0.4236757775,(MGRN1_XP_005706327.1_Galdieria_sulphuraria:4.1659250600,MGRN1_XP_005536920.1_Cyanidioschyzon_merolae:3.2719392440)92:1.4899541461)54:0.3940419836)48:0.3068887302,(MGRN1_CEO98225.1_Plasmodiophora_brassicae:3.6368224377,MGRN1_XP_002676307.1_Naegleria_gruberi:4.8727155631)94:1.1899609077)36:0.1822088386)78:0.1936497834,(((MGRN1_XP_001443657.1_Paramecium_tetraurelia:5.0710744593,MGRN1_XP_001025361.3_Tetrahymena_thermophila:4.9804036755)86:0.7319329411,MGRN1_EJY88708.1_Oxytricha_trifallax:5.1625158756)86:1.1676874607,((((MGRN1_EPY43869.1_Angomonas_deanei:0.5516396833,(MGRN1_XP_015657042.1_Leptomonas_pyrrhocoris:0.6159047219,MGRN1_CCW69607.1_Phytomonas_sp.:0.4633390492)100:0.1611523546)100:0.6005248731,MGRN1_XP_815262.1_Trypanosoma_cruzi:0.6064438770)100:4.9327798931,(MGRN1_XP_953663.1_Theileria_annulata:5.0422314388,MGRN1_XP_012766930.1_Babesia_bigemina:4.0314832781)99:2.2203882408)84:0.9561853312,MGRN1_XP_012895226.1_Blastocystis_hominis:6.2068238081)59:0.0855120691)64:0.3231918371)60:0.2626447148,(((MGRN1_XP_847288.1_Trypanosoma_brucei:1.2783452619,MGRN1_XP_009310993.1_Trypanosoma_grayi:1.0496530144)100:0.7271364166,(MGRN1_EPY22903.1_Strigomonas_culicis:2.7318592994,(MGRN1_KPI86947.1_Leptomonas_seymouri:1.2291044873,MGRN1_XP_001463767.1_Leishmania_infantum:1.1355401363)100:1.2104190489)100:0.6619769589)100:5.7799142426,MGRN1_OMJ90811.1_Stentor_coeruleus:4.0533298055)83:0.9350947891);